

# Targeting Macrophages and Synoviocytes Intracellular Milieu to Augment Anti-Inflammatory Drug Potency

Virgínia M. Gouveia,\* Loris Rizzello, Bruno Vidal, Claudia Nunes, Alessandro Poma, Ciro Lopez-Vasquez, Edoardo Scarpa, Sebastian Brandner, António Oliveira, João E. Fonseca, Salette Reis, and Giuseppe Battaglia\*

Using a preclinical in vivo model of arthritis and the gold standard disease-modifying anti-rheumatic drug, methotrexate, pH-responsive phosphorylcholine polymersomes, elicit both anti-inflammatory and anti-arthritic therapeutic efficacy, while drastically minimizing off-target toxicity. First, the selective accumulation of polymersomes within synovium of inflamed joints. Second, the polymersomes targeting ability toward activated macrophages and synoviocytes, via scavenger receptors, allow their uptake via endocytosis. And third, the polymersomes pH-responsiveness enables the drug escape from early endosomes and hence its intracellular milieu delivery. On-site augment of methotrexate loaded polymersomes enable the complete abrogation of synovial inflammation and prevent the disease progression and severity. Overall, in vitro and in vivo investigations reveal the potential of polymersomes as a promising nanotherapy for treating arthritic inflammation.

both pro- or anti-inflammatory actions depending on their surrounding feedback, such process is referred to as polarization. Often macrophages differentiate plastically from a M1 phenotype (pro) at the initial stages of inflammation resolution to M2 (anti).<sup>[1]</sup> Macrophage polarization is a critical step in resolving inflammation and promoting tissue repair, and any variations in its sequences give rise to immunological disorders.<sup>[1]</sup> In these are included the autoimmune diseases, chronic inflammatory conditions, immune-related deficiency syndromes, and even cancer. One of the most common chronic inflammatory autoimmune diseases is rheumatoid arthritis (RA).<sup>[2–4]</sup> RA is characterized by the progressive inflammation of the synovial tissue that causes cartilage damage and bone

erosion.<sup>[3–6]</sup> Disease pathogenesis involves the interplay of both innate and adaptive immune responses.<sup>[6–8]</sup> The influx of immune cells to the synovium and subsequent interacting cascades of pro-inflammatory cytokines causes synovitis.<sup>[6–8]</sup> Local cellular interactions initiate and maintain inflammation within the synovium, leading to an increased vascular permeability, which in turn leads to synovial hyperplasia and formation of


## 1. Introduction

Macrophages are one of the most important cells of the immune system and, as such, they are present in most organs adapting to the local environment, patrolling it from external attack. They are the main modulators of inflammation and so the primary immune response to cellular damage. Macrophages have

V. M. Gouveia, L. Rizzello, A. Poma, C. Lopez-Vasquez, E. Scarpa, G. Battaglia  
Department of Chemistry  
University College London  
London WC1H 0AJ, UK  
E-mail: virginia.mgouveia@somaserve.com; g.battaglia@ucl.ac.uk  
V. M. Gouveia, C. Lopez-Vasquez, G. Battaglia  
Institute of Physics of Living Systems  
University College London  
London WC1H 0AJ, UK

V. M. Gouveia  
SomaServe Ltd  
Babraham Research Campus, Cambridge CB22 3AT, UK  
V. M. Gouveia, C. Nunes, S. Reis  
LAQ  
REQUIMTE  
Department of Chemical Sciences  
Faculty of Pharmacy  
University of Porto  
Porto 4050-313, Portugal  
V. M. Gouveia, A. Oliveira  
Abel Salazar Biomedical Sciences Institute  
University of Porto  
Porto 4050-313, Portugal

L. Rizzello, G. Battaglia  
Institute for Bioengineering of Catalonia (IBEC)  
The Barcelona Institute of Science and Technology  
Barcelona 08028, Spain  
L. Rizzello, E. Scarpa  
Department of Pharmaceutical Sciences  
University of Milan  
Milan 20133, Italy

 The ORCID identification number(s) for the author(s) of this article can be found under <https://doi.org/10.1002/adtp.202100167>

© 2022 The Authors. *Advanced Therapeutics* published by Wiley-VCH GmbH. This is an open access article under the terms of the Creative Commons Attribution License, which permits use, distribution and reproduction in any medium, provided the original work is properly cited.

DOI: 10.1002/adtp.202100167

pannus tissue.<sup>[9,10]</sup> Among the cells found in the synovium, macrophages play a central role in RA pathogenesis by actively driving the perpetuation of immune and inflammatory responses and further damage of joint synovial tissue.<sup>[6,7,11–13]</sup> Macrophages induce the secretion of several pro-inflammatory cytokines, such as, tumor necrosis factor (TNF $\alpha$ ), interleukin (IL)1 $\beta$  and IL6, and chemokines, such as, CXCL8 (i.e., IL8) and CCL3 (also known as macrophage inflammatory protein 1 $\alpha$ ).<sup>[6–8,12,13]</sup> Through cascades of inflammation-mediated signaling pathways, activated macrophages trigger other cells, namely, the synoviocytes, to produce more pro-inflammatory cytokines and chemokines, thus perpetuating synovial inflammation and the disease progression.<sup>[6–8,11,12]</sup> Synoviocytes are important in the maintenance of the normal stromal synovial environment of joints through the secretion of a range of extracellular matrix components.<sup>[6,11,14–16]</sup> The inflammatory phenotype activation of synoviocytes leads to the secretion of tissue-degrading enzymes, such as, the matrix metalloproteinases (MMPs) that are involved in the degradation of cartilage.<sup>[6,11,14–16]</sup> In addition, the synoviocytes secrete the receptor activator of nuclear factor- $\kappa$ B (NF- $\kappa$ B) ligand (RANKL), which, in turn, induce the differentiation and proliferation of osteoclasts that are mainly responsible for bone erosion.<sup>[6,11,14–16]</sup> Moreover, synoviocytes play an important role in regulating the disease progression through the secretion of vascular endothelial growth factors associated with angiogenesis.<sup>[9,10,16–19]</sup> The enhanced synovial vascularization and prominent angiogenesis endures synovitis and facilitates the access of synoviocytes to the bloodstream, hence increasing the dissemination of arthritic inflammation to other unaffected joints.<sup>[9,16–18,20]</sup>

At an early stage, the disease manifestations include synovitis, erythema, swelling, and stiffness of affected joints.<sup>[6–8,21]</sup> Severe

disease progression can lead to the irreversible destruction of joints and hence loss of functionality.<sup>[6–8,21]</sup> RA is a serious unremitting health condition where early treatment intervention is crucial to slow down arthritis progression.<sup>[3–6,22]</sup> Despite the therapeutic advances, which focus mostly on the cease of synovial inflammation, methotrexate (MTX) still is the gold standard of currently used disease-modifying anti-rheumatic drugs in the treatment of RA, and other immunological disorders.<sup>[23]</sup> Different mechanisms of action are involved in the therapeutic effect of MTX, where the adenosine-mediated anti-inflammatory and immunosuppressive effects regulate the production of both cellular adhesion and pro-inflammatory molecules involved in inflammation.<sup>[24]</sup> Although, despite the therapeutic potency of MTX to control the disease inflammatory activity and hinder arthritis progression, a significant number of patients discontinue the therapy, mostly to deleterious adverse effects and intolerance.<sup>[25]</sup> In the last 15 years, several nanomedicines have been developed to improve MTX selective delivery in inflamed synovial tissues to overcome these limitations in clinic.<sup>[4,22,26]</sup> In this study, we propose the use of pH-responsive polymersomes, made of amphiphilic poly(2-(methacryloyloxy) ethyl phosphorylcholine)—poly(2-(diisopropylamino)ethyl methacrylate (PMPC–PDPA) polymer, as a promising drug delivery nanocarrier to target and treat arthritis. In vitro and in vivo findings presented here support the therapeutic potential of pH-responsive PMPC-PDPA polymersomes to control synovial inflammation and hinder arthritis progression. Beside their intrinsic strong stability, PMPC-PDPA polymersomes exhibited selective intracellular delivery of MTX in macrophages and synoviocytes, via scavenger receptors binding affinity endowed by the PMPC hydrophilic block.<sup>[27–29]</sup> Then, the PDPA hydrophobic block, carrying pH responsiveness to the acidic environment (typical of early endosomes) bestows the instant disassembly of polymersomes, allowing the MTX escape into cell milieu, where it acts.<sup>[27–29]</sup> We demonstrated that MTX-loaded polymersomes efficiently shut down the immune-mediated inflammatory response in vitro. And further validate their therapeutic impact in the progression of chronic synovial inflammation in well-established adjuvant-induced arthritis (AIA) animal model. In conclusion, we prove the beneficial therapeutic effect of pH-responsive PMPC-PDPA polymersomes in suppressing inflammatory arthritis progression, while minimizing off-target systemic exposure. Hence, establishing pH-responsive polymersomes potential to be used in the clinic for the treatment of RA as well as any other inflammatory immune-mediated disorders.

## 2. Results

### 2.1. Psomes as Suitable Drug Delivery Nanocarriers

Formulations of pH-responsive PMPC-PDPA polymersomes (subsequently designated psomes) and MTX-loaded psomes were successfully produced by pH-switch self-assembling methodology. Dynamic light scattering (DLS) measurements revealed that both formulations presented unimodal size distribution profiles with hydrodynamic diameters ( $D_h$ ) of  $93 \pm 13$  nm and  $96 \pm 11$  nm, respectively. Transmission electron microscopy (TEM) characterization also confirmed the spherical morphology of vesicles with a uniform size distribution of

L. Rizzello, E. Scarpa  
National Institute of Molecular Genetics (INGM)  
Milan 20122, Italy

A. Poma  
Division of Biomaterials and Tissue Engineering  
Eastman Dental Institute  
Royal Free Hospital  
UCL Medical School  
London NW3 2PF, UK

S. Brandner  
Department of Neurodegenerative Disease  
Queen Square Institute of Neurology  
University College London  
London WC1N 3BG, UK

B. Vidal, J. E. Fonseca  
Rheumatology Research Unit  
Institute of Molecular Medicine – IMM João Lobo Antunes  
Faculty of Medicine  
University of Lisbon  
Lisbon 1649-028, Portugal

J. E. Fonseca  
Serviço de Reumatologia  
Centro Hospitalar Universitário Lisboa Norte  
Centro Académico de Medicina de Lisboa  
Lisbon 1649-028, Portugal

G. Battaglia  
Catalan Institution for Research and Advanced Studies (ICREA)  
Barcelona 08010, Spain

about 90 nm (Figure S1A, Supporting Information). Likewise, TEM micrographs of both Cy5- and Cy7-psomes produced via solvent-switch present a homogeneous distribution of spherical polymersomes. The encapsulation of MTX was performed via modification of the pH-switch method. The drug was solubilized in a NaOH basic solution, rather than in the polymer solution at pH 2.0 before the self-assembly process. High-performance liquid chromatography (HPLC) quantifications confirmed the high drug loading capacity of psomes toward the MTX (up to  $18 \pm 2.1$  wt%; Figure S2, Supporting Information). This confirms the efficacy of the solvent switch method to enable a higher drug loading, possibly due to the affinity of MTX for the polymer during the self-assembly process. The partition coefficient value at pH 7.4 (log D of  $2.2 \pm 0.1$ ; Figure S3, Supporting Information) confirmed the affinity of MTX with the polymeric phase of the water/polymersome system. In vitro drug release studies were carried out overtime under physiologic and acidic pH conditions at 37 °C. The burst drug release profile observed at pH 5.0, with the complete release of MTX within 1 h incubation, confirmed psomes responsiveness to acidic pH in the intracellular endosomal compartments. Whereas we observed a more sustained drug release over time at pH 6.5 and negligible at pH 7.4, even after 50 h (Figure S4, Supporting Information). Drug release kinetic analyses based on the regression coefficient ( $r^2$ ) revealed that the best fitting model for pH 5.0 and pH 6.5 profiles was obtained by the Zero-Order and Higuchi models (Table S1, Supporting Information). These models suggest that the MTX release occurs through a controlled diffusion mechanism (Table S2, Supporting Information). In addition, and as expected, there was no best-fitted model for the release profile at pH 7.4 and practically negligible drug release was observed throughout 50 h (Figure S4, Supporting Information). These results demonstrate the effectiveness of psomes as a nanocarrier that ensures the loading of MTX and its on-site delivery.

## 2.2. Psores Biodistribution in Adjuvant-Induced Arthritis Rats

The biodistribution of psomes in the blood stream for 24 h was assessed to understand the pharmacokinetic behavior and stability in vivo. Two experimental groups of Wistar rats ( $n = 3$ ), one healthy and other with AIA, received an intraperitoneal (i.p.) injection of Cy7-psomes ( $10 \text{ mg kg}^{-1}$  body weight). Blood samples were then collected by tail vein puncture at different time points. The blood plasma concentration profile of injected Cy7-psomes, in both healthy and arthritic animal models, had two phases—absorption and elimination—characteristic of i.p. administration (Figure 1A and Figure S5A, Supporting Information). The absorption phase occurred within 2 h, reaching a maximum peak of psome concentration in the plasma of  $70 \pm 23 \mu\text{g mL}^{-1}$  (Figure 1A), followed by its elimination from the blood stream. We then analyzed the pharmacokinetic parameters of the Cy7-psomes in the plasma after i.p. injection in healthy and AIA Wistar rats (Figure 1B). The half-life ( $t_{1/2}$ ) of Cy7-psomes was calculated by one phase decay analysis of the elimination phase (dot line; Figure 1A). Despite the similarity of both plasma concentration-time profiles in the healthy and the AIA Wistar rats (Figure 1A; Figure S5A, Supporting Information), pharmacokinetic analysis resulted in a longer  $t_{1/2}$  and 2.5 times slower elimi-

nation rate ( $K_e$ ) in AIA rats relatively to healthy ones (Figure 1B). Also, the area under the curve for the AIA profile was greater than for healthy group (Figure 1B). These results suggest a longer circulation time of psomes in the bloodstream of AIA rats. Additionally, we studied the biodistribution of Cy7-psomes in various organs (spleen, kidneys, liver, and heart) in both healthy and arthritic Wistar rats. After 24 h from Cy7-psomes i.p. injection, all animals were euthanized and the organs were removed and wet weighed. The percentage of injected dose (%ID) per gram of tissue was then calculated by correlating the intensity of fluorescence of Cy7-psomes measured to the total weight of each organ. The analysis revealed high amounts of Cy7-psomes in the spleen of both experimental groups:  $4.7 \pm 1.2$  and  $3.0 \pm 1.2\%$  for healthy and AIA, respectively (Figure S5B, Supporting Information). Conversely, the injected dose of Cy7-psomes that accumulated per gram of liver was only  $1.0 \pm 0.1$  and  $1.2 \pm 0.1\%$  for healthy and AIA rats, respectively (Figure 1C). Similarly, the amount of Cy7-psomes detected in heart and kidneys was negligible (Figure 1C). Besides the distribution in the main organs, it was important to assess psomes distribution in the paws of both healthy and arthritic animals in order to confirm the nanocarrier ability to preferentially target the areas of synovial inflammation. IVIS imaging analysis revealed that no fluorescence intensity was detected in the paws of healthy rats oppositely to the AIA group (Figure 1D). Interestingly, we also noticed that the fluorescence signal detected in the paws of arthritic rats was dependent on the degree of joint swelling/inflammation score (AIA section: increase from left to right; Figure 1D). Normalization of the fluorescence intensity signal to the vehicle treated control highlighted the significant differences between the healthy and AIA groups (Figure 1E). Thereby, we confirm that psomes ably accumulate in the inflamed joints of AIA rats.

## 2.3. Psores Enhanced Uptake by Macrophages and Synoviocytes

The in vitro cellular uptake of psomes was assessed using live confocal laser scanning microscopy (CLSM) in macrophages and synoviocytes before and after activation with lipopolysaccharide (LPS) or TNF $\alpha$ , respectively (Figure 2A–D). CLSM imaging analysis of activated macrophages revealed that the normalized fluorescence intensity signal of Cy5-psomes constantly increased in a time-dependent manner up to 10-h after incubation, followed by a plateau (Figure 2E). Conversely, CLSM imaging on activated synoviocytes resulted in a triphasic cell uptake profile (Figure 2F). First, there was an increase in the internalization of Cy5-psomes, followed by a plateau of 5 h and another increase of fluorescence intensity signal (of almost 100%). Oppositely, the uptake profile in non-activated synoviocytes suggest a slow internalization of psomes overtime reaching a plateau after 1 h of incubation (Figure 2F). Overall, we observed that there is a rapid and higher uptake of Cy5-psomes upon cells inflammation phenotype activation comparing with the non-activated ones over a period of 48 h (Figure 2E,F). Additional imaging analyses suggested that the fluorescence intensity of Cy5-psomes in LPS-activated macrophages was higher than in TNF $\alpha$ -activated synoviocytes (Figure 2E,F). This is not only due to the intrinsic professional phagocytic nature of macrophages,<sup>[30]</sup> but also possibly to the inherent binding affinity of the PMPC building

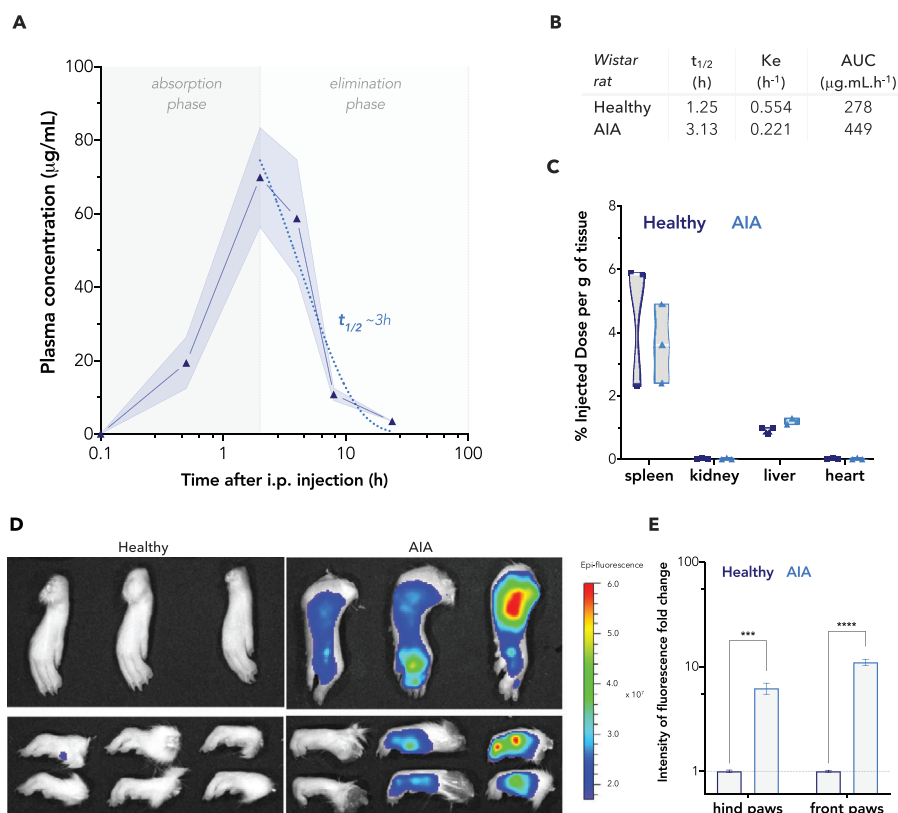


**Figure 1.** A) Plasma concentration-time profile of Cy7-psomes after i.p. injection in AIA Wistar rats. B) Pharmacokinetic parameters—terminal half-life ( $t_{1/2}$ ), elimination rate ( $K_e$ ), area under the curve (AUC)—regarding the plasma concentration-time profiles in healthy and AIA Wistar rats. C) The percentage of injected dose (%ID) of Cy7-psomes per gram of organ tissue weight after 24 h i.p. injection in healthy and AIA Wistar rats. D) IVIS images of the right hind (top) and front (bottom) paws of healthy and AIA rats. E) Fold change fluorescence normalized to the vehicle-treated control group. Data express the mean  $\pm$  SEM ( $n = 3$  per experimental group). The differences relative to healthy group were statistically significant for \* $p < 0.05$ , \*\* $p < 0.01$ , \*\*\* $p < 0.001$ , and \*\*\*\* $p < 0.0001$ .

block to the family of class B scavenger receptors, including type B1 and B3.<sup>[27]</sup> These surface cell receptors are expressed by both macrophages and synoviocytes.<sup>[29,31,32]</sup> We then used western blot analysis to investigate the protein expression levels of these scavenger receptors followed by cells activation (Figure S7A, Supporting Information). Results revealed that SRB1 and SRB3 (commonly known as CD36) expression levels in activated macrophages increased by two-fold and four-fold, respectively, compared to non-activated cells ( $p < 0.05$  and  $p < 0.01$ , respectively; Figure S7B, Supporting Information). Conversely, the activation of synoviocytes significantly boosted the expression of CD36 ( $p < 0.0001$  vs the non-activated control; Figure S7B, Supporting Information). However, the expression of SRB1 was only slightly increased in activated synoviocytes (Figure S7B, Supporting Information). The higher internalization of psomes by activated cells possibly occurs due to the high binding affinity of the PMPC moiety to overexpressed SRB1 and CD36. In turn, these surface cell receptors bestow the uptake of psomes via endocytosis and/or phagocytosis.<sup>[28,29]</sup> In addition, in vitro cytotoxicity studies assessed whether such increased uptake of psomes by activated macrophages and synoviocytes might affect cell viability. To this end, we carried out a 24-h MTT assay confirming the biocompatibility of psomes, as both cell types did

not show any considerable sign of cytotoxicity for concentrations up to  $0.6 \text{ mg mL}^{-1}$  (Figure S6A, Supporting Information). The loaded drug did not affect cell viability after 24 h incubation time (up to  $20 \mu\text{g mL}^{-1}$ ; Figure S6B,C, Supporting Information). Only the free MTX treatment displayed a concentration-dependent cytotoxicity, suggested by the sharp decrease on cell viability at the highest concentration (Figure S6B,C, Supporting Information).

#### 2.4. Psomes In Vitro Anti-Inflammatory Efficacy

In vitro cellular studies were carried out on activated macrophages and synoviocytes to evaluate the anti-inflammatory effect of MTX-loaded psomes in comparison concerning free drug treatment. To this end, we used CLSM to investigate the cellular localization of the transcription factor NF- $\kappa$ B. Activation of macrophages and synoviocytes in turn activates the NF- $\kappa$ B inflammatory signaling pathway. CLSM imaging analyses confirmed that upon cellular activation, NF- $\kappa$ B translocates from the cytosol to the nucleus, resulting in a marked fluorescence co-localization (quantified by the Pearson coefficient in Figure 3A,C). Quantitative co-localization imaging analyses demonstrated a twofold increase of the NF- $\kappa$ B nuclear translo-

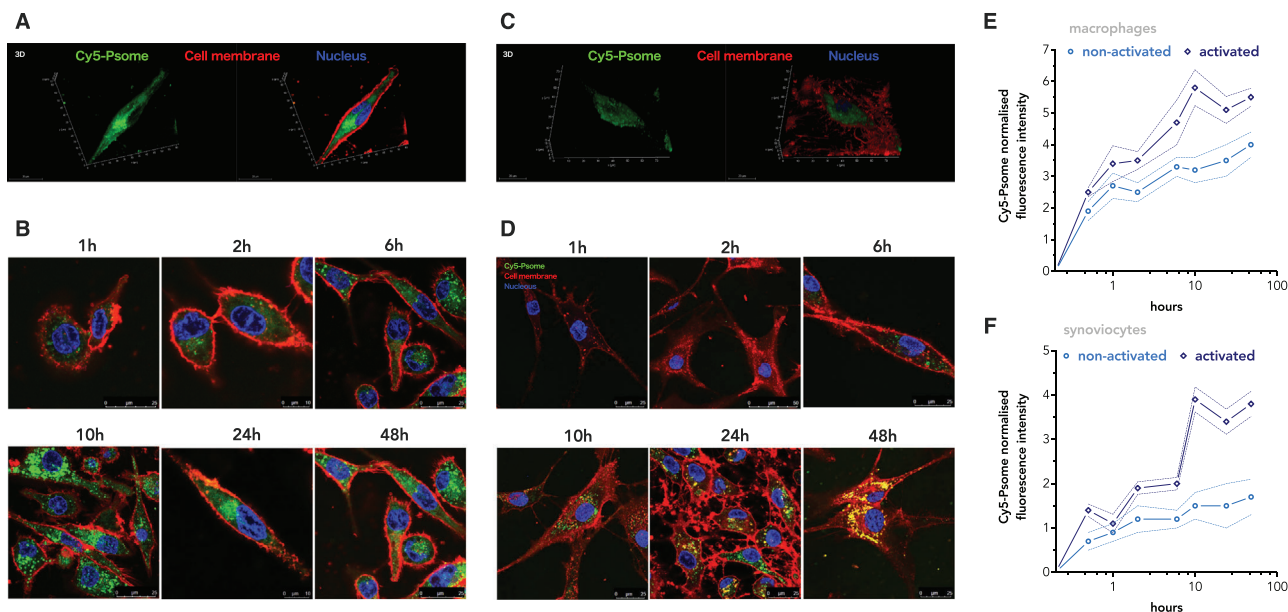


**Figure 2.** 3D and 2D CLSM images of Cy5-psomes (green fluorescence intensity signal) uptake by A,B) LPS-activated macrophages and C,D) TNF $\alpha$ -activated synoviocytes. Staining of the cell nuclei (blue fluorescence intensity signal) with Hoechst 33 342 and cell membrane (red fluorescence intensity signal) with far-red CellMask. E,F) Cell uptake profile of Cy5-psomes normalized fluorescent intensity relative to the nucleus signal measured as a function of time. Data express the mean  $\pm$  SEM (10 images for  $n = 2$ ).

cation on both activated cell types ( $p < 0.0001$  comparing with non-activated cells; Figure 3B). NF- $\kappa$ B is a key regulator of gene transcription in RA pathogenesis, with an important role in the production of pro-inflammatory mediators.<sup>[6,7,12]</sup> Thereby, inhibiting NF- $\kappa$ B translocation is a crucial step to regulate the inflammatory process. CLSM imaging co-localization analyses on both activated macrophages and synoviocytes demonstrated that a 24-h treatment with MTX-loaded psomes significantly reduced NF- $\kappa$ B translocation to the nucleus ( $p < 0.0001$  compared to activated control; Figure 3B). Nonetheless, both activated macrophages and synoviocytes treated with free MTX also showed a decrease nuclear translocation of NF- $\kappa$ B by 20% and 25%, respectively ( $p < 0.0001$  and  $p < 0.001$  compared to activated control; Figure 3B). Having demonstrated that both treatments inhibited the activation of the NF- $\kappa$ B signaling pathway, we evaluated the secretion levels of the key pro-inflammatory cytokine TNF $\alpha$  and IL6, which are involved in the synovial inflammatory response progression. We used ELISA to quantify their expression on activated macrophages and synoviocytes after 24 h treatment with increasing concentrations of either free or MTX loaded psomes. Both treatments reduced cytokine secretion levels in a concentration-dependent manner on activated macrophages (Figure 3D). MTX-loaded psomes showed a strong effect in reducing the secretion level of both cytokines, which could be possibly due to their enhanced internalization by activated macrophages (Figure 3D). This suggests that psomes enable the intracellular availability of MTX. In fact, even low concentrations of loaded MTX ( $2.5 \mu\text{g mL}^{-1}$ ) reduced TNF $\alpha$  levels by 1.5-fold compared with free drug treatment (Figure 3D). IL6 concentration was reduced to almost undetectable levels when activated macrophages were treated with MTX-loaded psomes at concentrations higher than  $2.5 \mu\text{g mL}^{-1}$ . Equal concentrations of the free drug resulted in approximately five-fold higher levels

of the same cytokine (Figure 3D). ELISA assays over activated synoviocytes also revealed that both treatments have the same effect on the secretion of TNF $\alpha$ , decreasing its concentration by nearly onefold compared to the non-treated control (i.e.,  $0 \mu\text{g mL}^{-1}$  of MTX; Figure 3E). IL6 secretion levels decreased in a concentration-dependent down to  $10 \mu\text{g mL}^{-1}$  in activated synoviocytes treated with MTX-loaded psomes, oppositely to free drug treatment that were maintained (Figure 3E). We then evaluated the expression of inflammation-related genes on both activated synoviocytes and macrophages by real-time quantitative polymerase chain reaction (RT-qPCR) after 24 h treatment with either free or MTX loaded psomes. Results confirmed that activation of macrophages and synoviocytes induces the up-regulation of all tested pro-inflammatory genes (control; Figure 3F,G). Conversely, treatment of activated macrophages with both free and loaded MTX significantly reduced the expression of all the cytokines and chemokines tested (Figure 3F). Both treatments also significantly reduced IL1 $\beta$ , IL6, and MMP13 gene expression levels on synoviocytes (Figure 3G). IL6 gene expression was significantly decreased on both cell types when treated with MTX-loaded psomes ( $p < 0.01$  and  $p < 0.0001$  comparing with the free drug-treated macrophages and synoviocytes, respectively; Figure 3F,G). These results demonstrate MTX-loaded psomes efficacy in reducing inflammation activity *in vitro*.

## 2.5. Posomes In Vivo Therapeutic Efficacy in Adjuvant-Induced Arthritis Rats

The AIA animal model has a rapid and severe disease progression following the administration of a foreign antigen of mycobacterial origin.<sup>[33,34]</sup> The joint swelling of the paws is indicative of RA progression and severity. At day 4 post disease

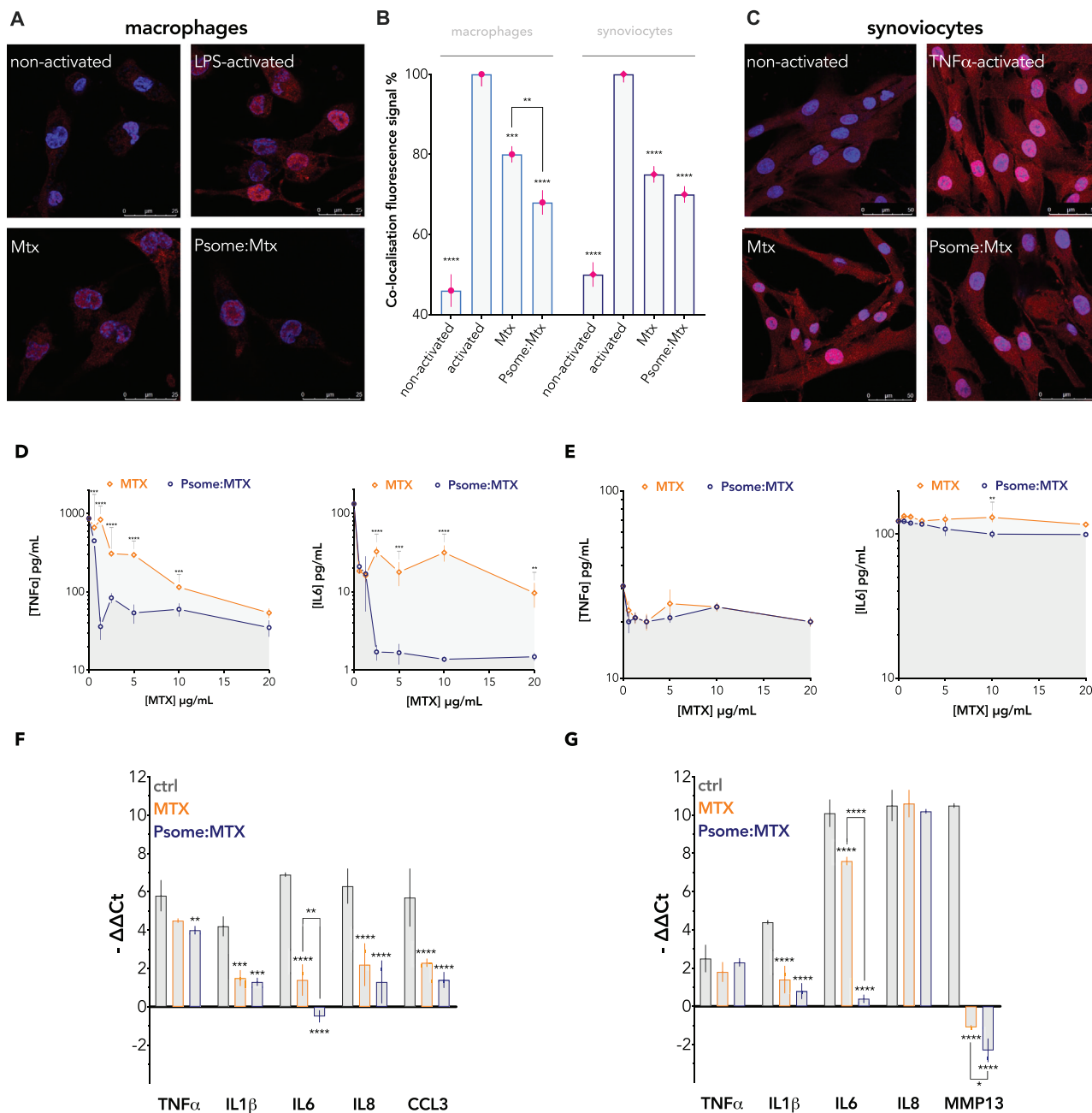


**Figure 3.** CLSM representative images of NF $\kappa$ B (red fluorescence intensity signal) translocation from cytoplasm to the nucleus (blue fluorescence intensity signal) on A) macrophages and C) synoviocytes. B) Co-localization fluorescence intensity signal (pink) analysis. Data express as mean  $\pm$  SEM (5 images for  $n = 2$ ). The statistically significant differences relative to activated control for  $*p < 0.05$ ,  $**p < 0.01$ ,  $***p < 0.001$ , and  $****p < 0.0001$ . ELISA analysis on the TNF $\alpha$  and IL6 protein secretion levels in D) LPS-activated macrophages and E) TNF $\alpha$ -activated synoviocytes. Data express as mean  $\pm$  SD ( $n = 3$ ). The statistically significant differences relative to MTX treatment for  $*p < 0.05$ ,  $**p < 0.01$ ,  $***p < 0.001$ , and  $****p < 0.0001$ . RT-qPCR on the gene expression levels in F) LPS-activated macrophages and G) TNF $\alpha$ -activated synoviocytes. Data express as mean  $\pm$  SD ( $n = 3$ ). The statistically significant differences relative to non-treated activated control for  $*p < 0.05$ ,  $**p < 0.01$ ,  $***p < 0.001$ , and  $****p < 0.0001$ .

induction, we observed that all hind paws of AIA Wistar rats developed arthritic inflammatory signs as evidenced by the visible erythema and swelling of the AIA joint (Figure 4A). In this animal model, all the arthritic inflammatory signs are severely increased over time, reaching the acute inflammation phase by day 13 post disease induction.<sup>[35]</sup> Indeed, we observed the rapid

symptomatic escalation after 10 days of treatment in the AIA group of animals (which also corresponds to the day 13 post induction; Figure 4B). Additionally, the maximal swelling of the paws, typical in arthritic animal models, occurs by day 19 post disease induction before reaching a plateau phase.<sup>[35]</sup> Taking this into consideration and having established the accumulation

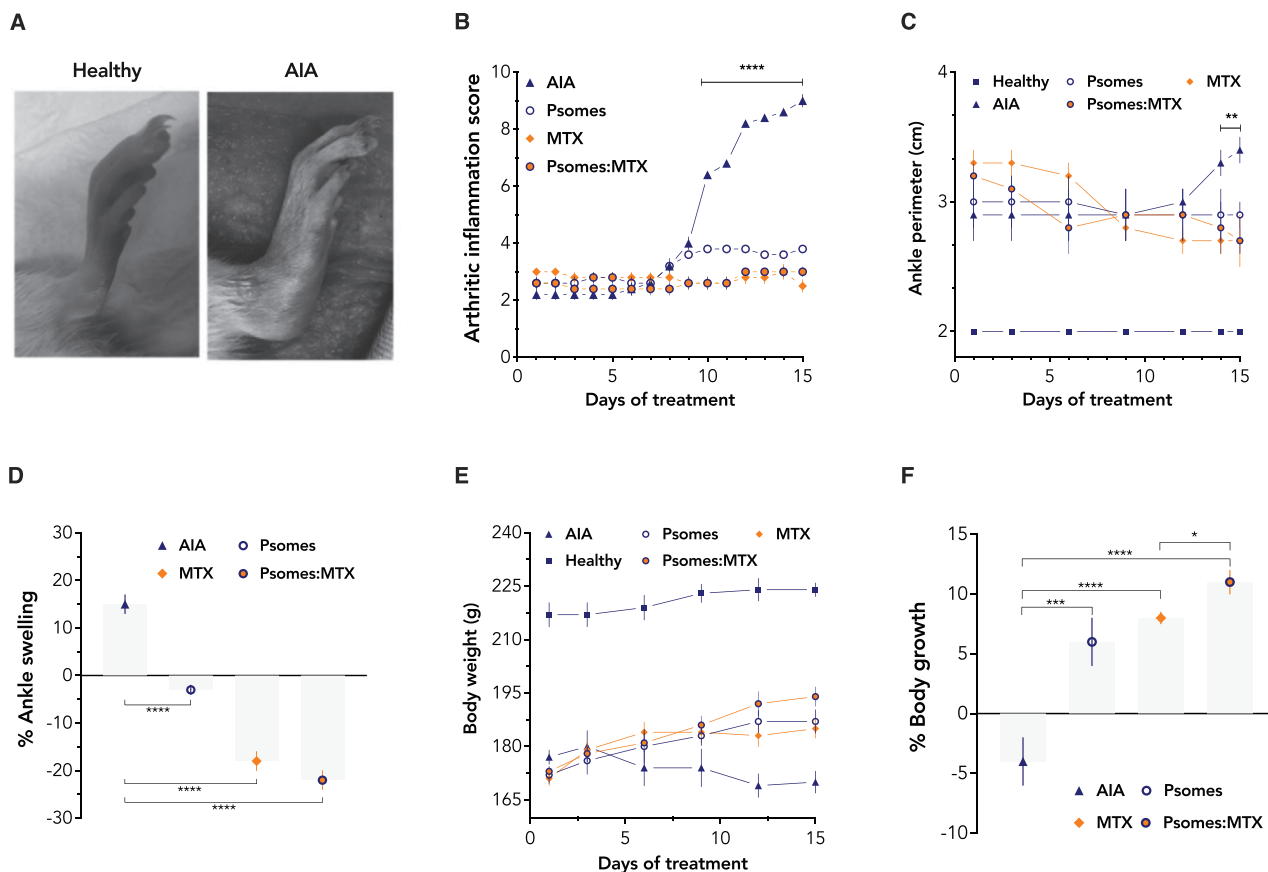


**Figure 4.** A) Representative images of the left hind paw of a healthy and AIA Wistar rat. B) Paws arthritic inflammation score over the 15 days period of treatment. Data defined as the mean  $\pm$  SEM of the sum of the partial scores of each affected joint. C) Ankle perimeter of hind paws and D) variation of the ankle swelling percentage over the 15 days of treatment. E) Body weight and F) variation of the body growth percentage over the 15 days of treatment. Data express the mean  $\pm$  SEM ( $n = 5$  per experimental group). Statistical analysis for  $*p \leq 0.05$ ,  $**p \leq 0.01$ ,  $***p \leq 0.001$ , and  $****p \leq 0.0001$ .

of psomes to inflamed synovial joints, the therapeutic efficacy of psomes to control the progression of arthritic inflammation was evaluated for 15 days of treatment in AIA rats (which corresponds the 4<sup>th</sup> and 19<sup>th</sup> days post disease induction time frame). To this end, the different groups of AIA rats were daily i.p. injected with either vehicle, MTX (i.e., free drug), MTX-loaded psomes or empty psomes. Then, all animals were monitored constantly for 15 days by evaluating the arthritic inflammation score, which is based on assessing the ankle swelling and body weight. We observed the continuous disease progression in AIA vehicle-treated rats by their body weight loss, the increased swelling of the joints and hence of the arthritic inflammation score (Figure 4B,C). Indeed, the AIA vehicle-treated group showed a significant increase of the ankle perimeter ( $p < 0.001$  comparing with the healthy control group where the arthritic inflammation score is 0; Figure 4C). Conversely, all the other treatments resulted in a decrease of inflammatory arthritic signs. We observed that AIA animals treated with either free or loaded MTX exhibited a significantly lower arthritic inflammation score than the psomes treatment group, especially in the last 5 days of treatment ( $p < 0.0001$ ; Figure 4B). The average ankle swelling of the MTX-loaded psomes, and MTX-treated groups was significantly reduced, respectively, by 22% and 19% relative to the first

day before treatment starts ( $p < 0.0001$  vs the AIA vehicle-group; Figure 4D). The paw swelling in AIA rats was reduced only by 4% the psomes treatment group, but still this represents a striking difference compared with the AIA rats by the end of 15 days ( $p < 0.0001$ ; Figure 4D). AIA rats receiving either free MTX or MTX-loaded psomes treatment resulted in the same degree of paw inflammation and swelling (Figure 4B–D). Moreover, we observed that AIA animals lost 6% of their weight since the beginning of treatment, oppositely to the MTX-loaded psomes group with 11% of body growth ( $p < 0.0001$ ; Figure 4E,F). The therapeutic effect of the different treatments in AIA rats joints was further evaluated using hematoxylin & eosin (H&E) histological assessment. The H&E imaging analysis of the AIA vehicle-treated animals showed signs of the early inflammatory process, such as immune cellular infiltration and proliferation, followed by formation of pannus (Figure 5A–C). Histological evaluation using semi-quantitative scores was performed to identify signs of cartilage degradation and bone erosion, also revealing that both scores were significantly increased in the AIA vehicle-treated group comparing with the healthy one ( $p < 0.0001$ ; Figure 5D,E). Conversely, H&E histopathological analyses of the AIA rat joints from either free or loaded MTX treatment groups resulted in a reduction of the sub-lining layer

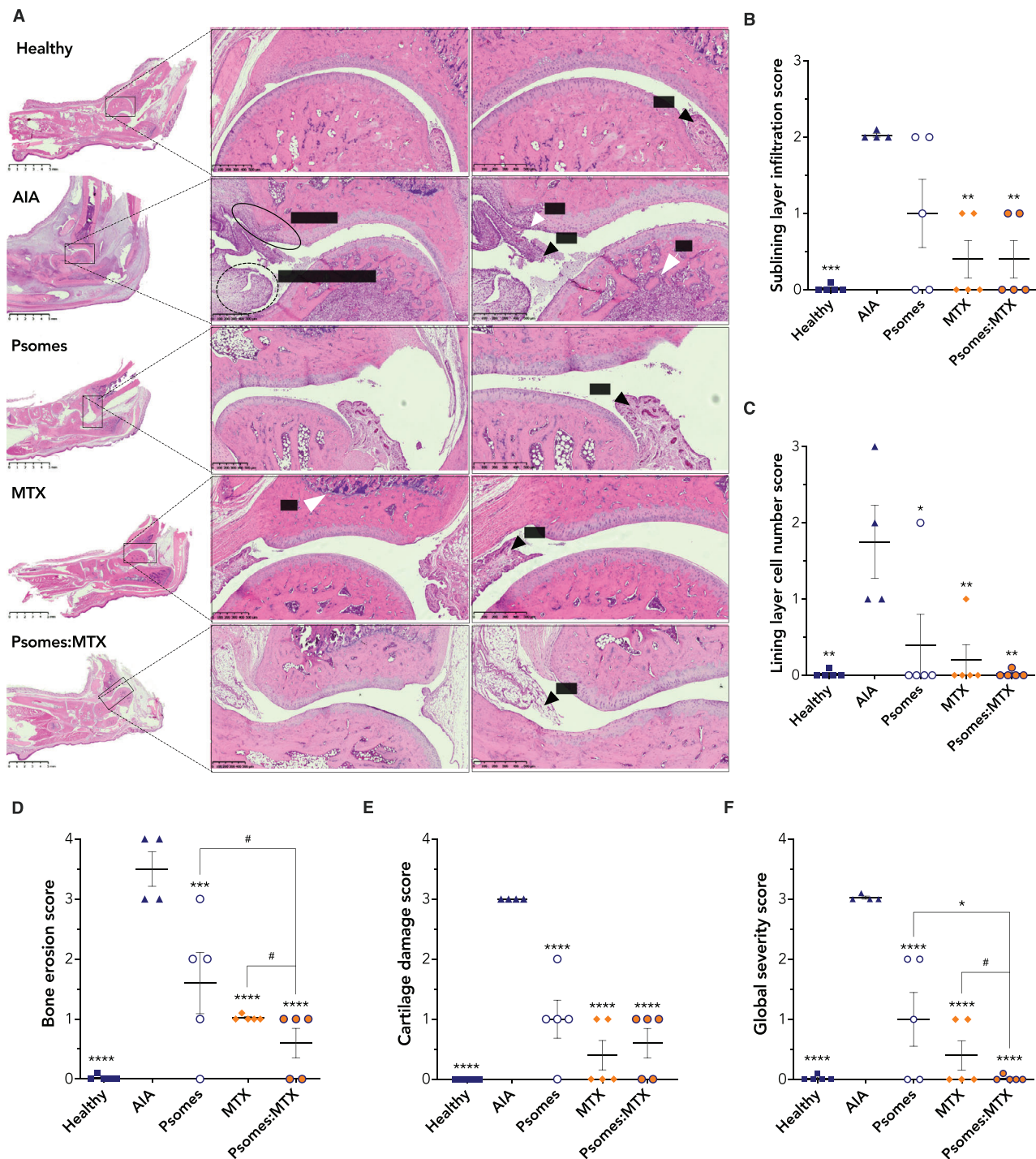


**Figure 5.** A) H&E histological representative images of the left hind paw of each experimental animal group (scale bar: 500  $\mu$ m; SM: synovial membrane; CD: cartilage damage; BE: bone erosion). Histological evaluation: B) Sublining layer infiltration score (0 = none to diffuse infiltration, 1 = lymphoid cell aggregate, 2 = lymphoid follicles, 3 = lymphoid follicles with germinal center formation); C) Lining layer cell number score (0 = fewer than three layers, 1 = three to four layers, 2 = five to six layers, 3 = more than six layers); D) Bone erosion score (0 = no erosions, 1 = minimal, 2 = mild, 3 = moderate, 4 = severe); E) Cartilage damage score (0 = normal, 1 = irregular, 2 = clefts, 3 = clefts to bone); F) Global severity score (0 = no signs of inflammation, 1 = mild, 2 = moderate, 3 = severe). Data express the mean  $\pm$  SEM. Statistical analysis versus the AIA experimental group (\* $p \leq 0.05$ , \*\* $p \leq 0.01$ , \*\*\* $p \leq 0.001$ , and \*\*\*\* $p \leq 0.0001$ ) and the psomes loading MTX group (# $p \leq 0.1$  and \* $p \leq 0.05$ ).



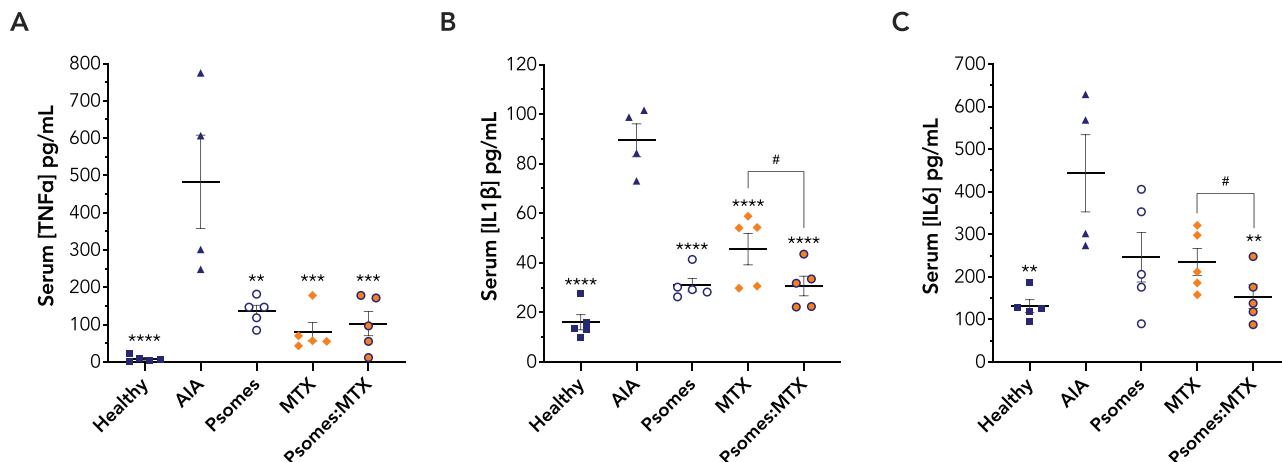


**Figure 6.** A) TNF $\alpha$ , B) IL1 $\beta$ , and C) IL6 protein levels in the serum of animals after the 15 days of treatment. Data express the mean  $\pm$  SEM ( $n = 5$ ). Statistical analysis versus the AIA experimental group ( $*p \leq 0.05$ ,  $**p \leq 0.01$ ,  $***p \leq 0.001$ , and  $****p \leq 0.0001$ ) and the psomes loading MTX experimental group ( $\#p \leq 0.1$ ).

infiltration score (Figure 5B) and number of lining layer of cells score compared to the arthritic group ( $p < 0.01$ ; Figure 5C). As a consequence of no apparent pannus formation, histological analyses of arthritic rats treated with MTX-loaded psomes showed a smooth cartilage surface and a reduced subchondral bone leukocyte infiltration (Figure 5E). Consistent with these results, treatment with MTX-loaded psomes was more efficient in reducing the bone damage ( $p < 0.1$  vs MTX-treated group; Figure 5D). Hence, negligible differences in the global disease severity score were observed in AIA rats administrated with the MTX-loaded psomes compared with the healthy rats (Figure 5F). Interestingly, i.p. injection of psomes also demonstrated to have a significant therapeutic effect in the arthritic animals, particularly in preventing bone and cartilage degradation ( $p < 0.001$  and  $p < 0.0001$  vs AIA vehicle-treated animals respectively; Figure 5D,E). Also, there was no visible inflammation in the paws for all the other treatments concerning the AIA group (Figure 5A). We also performed H&E histological assessment of all the livers and spleens to confirm the extent of any tissue damage or deleterious effect related to any treatment administrated. H&E revealed the characteristic liver architecture, with formation of lobules and normal lobular structure (Figure S8, Supporting Information), as well as, the characteristic follicular structure of the spleen can be identified (Figure S9, Supporting Information). MTX is well-known by causing severe side effects related to long-term systemic exposure.<sup>[25]</sup> And, indeed, in the livers of the MTX treated AIA rats (Figure S8D, Supporting Information), we observed signs of fibrosis and indefinitely giant cells, possibly accompanied by mild to moderate inflammation. More importantly, histopathological analysis confirms the absence of any sign of inflammation or tissue damage in the livers and spleens of AIA rats treated with either MTX-loaded psomes or empty psomes.

Additionally, to understand the efficacy of the different treatments in reducing systemic inflammation spreading in AIA rats, we investigate the levels of pro-inflammatory cytokines associated with disease activity in vivo. ELISA was used for the quantification of TNF $\alpha$ , IL1 $\beta$ , and IL6 in the serum of all animal groups after 15 days of treatment. The vehicle-treated AIA rats exhib-

ited high serum protein levels of TNF $\alpha$ , IL1 $\beta$ , and IL6, in comparison with the healthy control group ( $p < 0.0001$ ,  $p < 0.0001$ , and  $p < 0.01$ , respectively; Figure 6). Thereby, as expected, the arthritic group presented systemic inflammatory manifestations reflected by hyperplasia and synovial inflammation. In contrast, all tested inflammation-related cytokines levels decreased to a different extent in the three arthritic groups after 15 days of daily treatment. Both free MTX and MTX-loaded psomes treatments significantly decreased TNF $\alpha$  concentration in the serum by five-fold ( $p < 0.001$  vs AIA vehicle-treated group; Figure 6A). The serum levels of IL1 $\beta$  also decreased after treatment with both free and MTX-loaded psomes ( $p < 0.001$  and  $p < 0.0001$ , respectively; Figure 6B). Remarkably, psomes treated AIA rats reduced the pro-inflammatory cytokine levels, particularly for TNF $\alpha$  and IL1 $\beta$  ( $p < 0.01$  and  $p < 0.0001$ , respectively; Figure 6A,B). Serum concentration of IL1 $\beta$  were similar and for both psomes treatments when compared with the healthy control group (Figure 6B). We had shown in a previous in vitro study that PMPC-PDPA polymersomes effectively inhibit inflammatory pathways signaling and suppress the production of TNF $\alpha$ , IL1 $\beta$ , and IL6 by LPS-activated macrophages.<sup>[36]</sup> Additional analyses suggest that MTX-loaded psomes were more effective in reducing the IL1 $\beta$  and IL6 levels in serum than conventional MTX treatment ( $p < 0.1$  for both; Figure 6B,C). Increased values of serum IL6 were also observed in the vehicle-treated AIA group, which have shown bone loss evidence in the histological analyses (Figure 5A,D). By the end of 15 days, the IL6 concentration of the MTX-loaded psomes treatment group was significantly reduced to  $154 \pm 28$  pg mL $^{-1}$  ( $p < 0.01$  vs AIA vehicle-treated group; Figure 6C), which was similar to the healthy vehicle-treated rats ( $131 \pm 15$  pg mL $^{-1}$ ). Thereby, reduced levels of these inflammation-mediated cytokines demonstrate the MTX-loaded psomes potential to suppress both local and systemic inflammation in AIA treated rats.

### 3. Discussion

In this study, we investigate the therapeutic potential of pH-responsive PMPC-PDPA psomes in the treatment of inflam-

matory arthritis by targeting macrophages and synoviocytes intracellular milieu to augment on-site MTX potency.

Starting with in vivo biodistribution studies, we demonstrate the effectiveness of the nanometric size and spherical morphology of psomes to facilitate their passive accumulation within inflamed joints of AIA rats. This is most likely due to the prominent angiogenesis and enhanced vascularization of inflamed synovial tissues and their enhanced permeation and retention effect toward nanocarriers.<sup>[9,10,17,19,37,38]</sup> Additional pharmacokinetics analyses demonstrated the robust properties and stability of psomes in vivo upon i.p. injection. This is ascribed to psomes biocompatibility and to their PMPC hydrophilic building block, which hinders protein fouling in the bloodstream and avoids a mononuclear phagocyte system-based clearance.<sup>[27]</sup> The accumulation of psomes in the liver and spleen of rats can be explained by the i.p. injection, which induces drugs entering the portal vein and pass through the liver before accessing the bloodstream. Also, these organs are the main routes of excretion for nanocarriers.<sup>[39]</sup> More importantly, liver and spleen histopathological analyses confirm that none of the treatments with psomes cause any tissue damage. Biodistribution studies are also indicative of psomes ability to improve the on-site bioavailability and activity of loaded MTX within synovial disease-inflamed tissues of joints. Here, macrophages and synoviocytes found in the synovium of joints are key targets for MTX delivery, particularly due to their important role in RA pathogenesis.<sup>[6–8,11,12,15]</sup> The activation of the macrophages inflammatory phenotype induces the secretion of key pro-inflammatory mediators since the early disease stages, which are involved in the maintenance and perpetuation of the synovial inflammatory response.<sup>[6,7,12]</sup> On the other hand, synoviocytes take on a more aggressive and invasive phenotype that drives the joint destruction process.<sup>[6,11,14–16]</sup> Not only we demonstrate psomes accumulation in the inflamed joints of AIA rats, but also with the in vitro cellular uptake studies, we prove their enhanced targeting ability toward activated macrophages and synoviocytes intracellular milieu. We also show that this enhanced internalization is not only ascribed to the nanometric size of psomes,<sup>[40]</sup> but mostly to the PMPC building block inherent binding affinity to the family of class B scavenger receptors, including type B1 and B3 overexpressed on these cells.<sup>[27,36,41,42]</sup> Upon cellular internalization, in vitro drug release study confirms the acidic pH responsiveness-trigger mechanism of psomes hydrophobic PDPA building block to bestow their rapid disassemble along the endocytic pathway.<sup>[27,28,36,38,41–43]</sup> This enables an efficient delivery of the loaded MTX within early endosomes (pH  $\approx$  6 to 5) and eventual escape into the cytosol, as a result of the osmotic shock in the endosome and consequent membrane poration.<sup>[27,28,36–38,41–43]</sup> In addition, this mechanism can be further exploited as a targeting strategy for RA, as the acidic environment within the synovium leads to a pH drop, thus allowing the release of loaded MTX in the target inflamed synovial tissues.<sup>[19,44]</sup>

Further in vitro cellular studies gave insight into the activation of macrophages and synoviocytes as a result of the NF- $\kappa$ B nuclear translocation signaling and up-regulation of pro-inflammatory genes involved in the progression of chronic synovial inflammation. Additionally, we demonstrate the anti-inflammatory potential of MTX-loaded psomes in inhibiting the NF- $\kappa$ B signaling pathway and in modulating the expression of pro-inflammatory

cytokines and chemokines. Among these, IL6 mediates both innate and adaptive immune system activation, together with TNF $\alpha$  and IL1 $\beta$ , since the early acute inflammatory state of the disease.<sup>[6,7,12,45,46]</sup> Therefore, down-regulation of IL6 and IL1 $\beta$ , observed on both activated macrophages and synoviocytes, is crucial to prove psomes treatment anti-inflammatory efficacy. Moreover, the immunosuppressive effect of MTX-loaded psomes was further demonstrated by the reduced expression levels of IL8 and CCL3 genes on activated macrophages. These chemokines are involved in the acute inflammation phase of RA mediating the recruitment and activation of immune cells to the synovium.<sup>[6,7,12,47]</sup> Further confirmation of the potential efficacy of MTX-loaded psomes in shutting down the joint destructive process in RA results from the down-regulation of MMP13 gene expression on activated synoviocytes. As synoviocytes activation induces the production of these metalloproteases responsible for the cartilage damage.<sup>[6,7,12,14–16]</sup> Also, inactivation of the NF- $\kappa$ B nuclear translocation on activated synoviocytes might have an impact on bone erosion because RANK (which induces osteoclast activation) is regulated by NF- $\kappa$ B-dependent signaling.<sup>[6,7,11,12,14–16]</sup> Hereby, we prove in vitro that MTX-loaded psomes promote inflammation resolution at the molecular level.

As the disease progresses, synovial hyperplasia and chronic synovial inflammation eventually lead to the irreversible joint destruction.<sup>[11,48]</sup> Psomes were evaluated for their anti-inflammatory and anti-arthritic therapeutic efficacy in vivo by assessing the arthritic inflammation signs and the histopathological features of joints of AIA-treated rats. In vivo studies revealed the therapeutic potential of MTX-loaded psomes in the abrogation of disease progression and severity. Clinical arthritic inflammation signs and histopathological analyses on AIA rats treated with MTX-loaded psomes resulted in the suppression of synovial inflammation and also in the complete abrogation of joint synovial hyperplasia, and hence prevented cartilage and bone damages. The on-site augment of MTX is fundamental for its therapeutic efficacy. Hence, the anti-rheumatic and -inflammatory therapeutic effect of psomes mostly results from their facilitated accumulation within synovial tissues of inflamed joints. Though, we also show that MTX treatment had similar beneficial therapeutic effect in the inhibition of the inflammatory joint signs. The timing and dosing of administrated MTX administrated are also key parameters to understand the extent of treatments efficacy, due to the drug's rapid clearance and hence its well-known hepatotoxicity.<sup>[25]</sup> And, in fact, histopathological analyses on AIA rats treated with MTX-loaded psomes did not show any liver damage even after daily administration for 15 days. Oppositely to the MTX treatment, in which the rat's livers present signs of fibrosis and mild inflammation. Therefore, we show that MTX-loaded psomes can abrogate arthritic inflammation, while minimizing the well-known hepatotoxicity of this potent anti-rheumatic drug, that often hinders its continuity in clinic for RA treatment.

In addition, we demonstrated the efficacy of MTX-loaded psomes to inhibit systemic inflammation spreading in AIA animals by analyzing serum levels of pro-inflammatory cytokines. In RA, synovial inflammation progresses through interacting cascades of pro-inflammatory cytokines. TNF $\alpha$ , IL1 $\beta$ , and IL6 are reported to be inherently associated with systemic and local inflammations in patients with RA.<sup>[6,7,11,12]</sup> TNF $\alpha$  and IL1 $\beta$  are believed

to play an important role since the early phase of the disease as they directly stimulate the infiltration of leucocytes, neutrophils, and macrophages into the synovium.<sup>[6,7,11,12]</sup> As mentioned before, IL6 is involved in the perpetuation of synovial inflammation together with IL1 $\beta$  and TNF $\alpha$ , but it plays also a key role in the progressive damage of joints.<sup>[6,7,11,12,45,46]</sup> IL6 activates the synoviocytes to release metalloproteases and reactive oxygen species, leading to the destruction of the cartilage tissue.<sup>[6,7,11,12,15,45]</sup> This cytokine is also involved in osteoclast differentiation and activation, which are mostly responsible for bone erosion.<sup>[6,7,11,12,15,45]</sup> Remarkably, psomes alone can hinder arthritic progression, as well as be effective in the suppression of systemic inflammation signs in AIA model of arthritis. Previous reports ascribed the anti-inflammatory action of phosphatidylcholine psomes to their enhanced internalization through the cell scavenger receptor class B type 1, which, in turn, is involved in the regulation of intracellular inflammatory pathways.<sup>[32,36,49]</sup> Additionally, the safety and biocompatibility of psomes in prolonged administration must be guaranteed, as they should not cause any cytotoxic, inflammatory, or immunogenic effects. To this respect, we showed the biocompatibility of psomes in vivo, as no subacute systemic toxicity was observed after 15 days of daily treatment. Overall, in vivo studies confirm the beneficial impact of MTX-loaded psomes to control the progression of both local and systemic inflammatory arthritis, as well as, to hamper the disease destructive process with minor deleterious off-target toxicity.

#### 4. Conclusion

In conclusion, in vitro and in vivo studies support the hypothesis that MTX-loaded psomes exhibit an effective anti-arthritic and anti-inflammatory therapeutic impact with significant amelioration of synovial inflammation and complete abrogation of joint destruction. Posomes targeting ability toward activated macrophages and synoviocytes intracellular milieu augment the potency of loaded MTX to shut-down inflammation on-site and, hence impede arthritis progression, while minimizing its well-known hepatotoxicity that often hinders the effectiveness of conventional RA treatment.

#### 5. Experimental Section

**Preparation and Characterization of Posomes:** Polymersomes formulations are made of amphiphilic PMPC-PDPA polymer (Figure S1B, Supporting Information) designed to self-assemble into vesicles in aqueous conditions at pH above 6.2 (the PDPA pKa).<sup>[36,41,43,50]</sup> Formulations of PMPC-PDPA polymersomes (i.e., psomes) were then prepared using a previously reported pH-switch method with some modifications.<sup>[51,52]</sup> Briefly, under sterile conditions, PMPC<sub>25</sub>-PDPA<sub>68</sub> polymer, previously synthesized by atom-transfer radical polymerization,<sup>[53]</sup> was dissolved in acidic phosphate-buffered saline (PBS 0.1 M at pH 2.0, Sigma-Aldrich) up to a concentration of 10 mg mL<sup>-1</sup>. The pH-driven self-assembly process was controlled by increasing the solution pH from 2.0 to approximately neutral pH 7.4, through an injection system (2 mL min<sup>-1</sup>) of sodium hydroxide (NaOH 0.5 M at pH  $\approx$  14). Formulations of psomes loaded with methotrexate (MTX, C<sub>20</sub>H<sub>22</sub>N<sub>8</sub>O<sub>5</sub>, MW 454.44,  $\lambda$  (300 nm), Sigma-Aldrich) were prepared also using the above-mentioned pH-switch method by injecting the MTX (3 mg mL<sup>-1</sup>) dissolved together in the NaOH solution. Additionally, for fluorescence imaging purposes either Cyanine5- or Cyanine7-labelled psomes were prepared using the solvent-switch method as reported with

some modifications.<sup>[54]</sup> Briefly, 10% (w/w) Cy5- or Cy7-PMPC<sub>25</sub>-PDPA<sub>68</sub> copolymer was dissolved together with the PMPC<sub>25</sub>-PDPA<sub>68</sub> in an organic solution of 3:1 (v/v) methanol:tetrahydrofuran (Sigma-Aldrich) for a final copolymer concentration of 20 mg mL<sup>-1</sup>. Then, PBS at pH 7.4 was added into the copolymer solution under constant stirring at 42 °C, through needle injection system at the rate of 2 mL min<sup>-1</sup>, until a 0.6% (w/v) PBS content was reached. Finally, any remained organic solvent was removed by dialysis (3.5 kD MWCO tubing membrane, Spectrum Labs) against PBS for 2 days. Afterward, all formulations were purified, as previously described by size exclusion chromatography, and characterized in terms of size, size distribution, and morphology.<sup>[52]</sup> DLS technique was used for the hydrodynamic size measurements in the Zetasizer Nano ZS (Zen1600, Malvern Instruments), equipped with a 633 nm HeNe laser in a scattering angle of 173°. Additionally, the morphology was accessed by transmission electronic microscopy (TEM) using a JEOL 2100 operating at 200 kV, equipped with an Orius SC2001CCD Gatan camera. Prior to DLS and TEM characterization, all samples were respectively prepared as previously reported.<sup>[36,55]</sup> Follow the purification process, the psomes drug loading capacity, estimated as the number of MTX molecules per psome, was determined using a previously reported method,<sup>[36,50]</sup> after measurement on the amount of PMPC<sub>25</sub>-PDPA<sub>68</sub> copolymer and loaded MTX by HPLC (Dionex Ultimate3000, Thermo Scientific).

The drug-polymer interaction study was performed by determining the partition coefficient (expressed as  $K_p$  and log D) of MTX in a polymersomes/water system. A previously reported method of derivative spectrophotometry,<sup>[56]</sup> was used with some modifications, to determine the  $K_p$  of MTX with the polymeric membrane at pH 7.4 and 37 °C. Briefly, samples with increasing concentrations of psomes (0–120  $\mu$ M) and a fixed concentration of MTX (25  $\mu$ M) at pH 7.4 were prepared and incubated for 1 h. The absorption spectra (220–370 nm) were obtained at 37 °C using a UV–vis microplate spectrophotometer (Synergy HT, Biotek). The obtained experimental data were mathematically analyzed using a previously reported  $K_p$  calculator.<sup>[56]</sup> The second-derivative spectra were used to eliminate the light scattering effect caused by the polymersomes and improve bands resolution. Hence, by plotting the second-derivative values, at a wavelength where the scattering was eliminated ( $\lambda_{min} \approx$  255 nm), as a function of the psomes molar concentrations, the  $K_p$  (M<sup>-1</sup>) was determined by fitting the experimental data using a nonlinear least-squares regression method.<sup>[56]</sup> Results on the drug interaction with the water/polymer system are expressed as log D (details in Figure S3, Supporting Information). The drug release study was performed using the dialysis method under sink conditions. As previously described,<sup>[36]</sup> 1 mL of MTX-loaded psomes or free MTX (at the same concentration of the loaded one) was filled in a cellulose ester dialysis membrane tube (3.5–5 kDa MWCO, Float-a-Lyzer G2, Spectrum Laboratories Inc.). These dialyses were carried out against 10 mL of three different outer buffer pH conditions (PBS at pH 7.4; acetate-buffered solution at pH 6.5 or 5.0) for 50 h under continuous magnetic stirring at 37 °C (RT15 power, IKA-Werke GmbH & Co. KG). At regular time points, aliquots (200  $\mu$ L) were withdrawn, and the same volume of respective fresh outer buffer solution replaced to maintain the sink conditions. The quantification of permeated drug aliquots throughout the 50 h was determined by measuring the UV absorbance of MTX at  $\lambda$  (300 nm) using the UV–vis microplate spectrophotometer (Synergy HT, Biotek). Mathematical models for drug-release kinetics, including zero-order and first-order equations, Higuchi and Hixson-Crowell models, were applied to each drug release profile to evaluate the mechanism of drug release.<sup>[36,50]</sup> The fitting of each model was evaluated based on the correlation coefficient ( $r^2$ ) values (details in Table S1, Supporting Information).

**Cell Culture and Activation:** Human leukemic monocytes (THP-1) were cultured and maintained in RPMI-1640, 2 mM L-glutamine, 25 mM Hepes (Sigma-Aldrich) supplemented with 10% (v/v) heat-inactivated fetal bovine serum (FBS, Sigma-Aldrich), 1% (v/v) penicillin-streptomycin (Sigma-Aldrich), and 0.1% (v/v) amphotericin B (Sigma-Aldrich). Human fibroblast like synoviocytes (HFLS) purchase from Sigma-Aldrich were cultured and maintained in synoviocytes growth medium (Sigma-Aldrich) supplemented with 10% (v/v) FBS, 1% (v/v) penicillin-streptomycin, 1% (v/v) L-glutamine (Sigma-Aldrich), and 0.1% (v/v) amphotericin B. Prior

to all in vitro cellular studies, THP-1 cells differentiation into mature macrophages-like state was induced through incubation with 10 ng mL<sup>-1</sup> of phorbol 12-myristate 13-acetate (PMA, Sigma-Aldrich) for 48 h in a humidified atmosphere, 95% air, 5% CO<sub>2</sub> at 37 °C.<sup>[36,57]</sup> Moreover, unless stated otherwise, macrophages pro-inflammatory M1 phenotype activation was induced with 600 ng mL<sup>-1</sup> of LPS (Sigma-Aldrich);<sup>[36,57]</sup> while, HFLS activation was induced with 20 ng mL<sup>-1</sup> of TNF $\alpha$  (Sigma-Aldrich).<sup>[58]</sup> Follow by 24 h incubation in a humidified atmosphere, 95% air, 5% CO<sub>2</sub> at 37 °C.

**Cell Uptake Imaging:** The cell uptake imaging was performed using CLSM (Leica SP8). First, THP1 and HFLS were seeded at a concentration of 5 × 10<sup>4</sup> cells per glass-bottom petri dish (Ibidi) and then activated to the inflammatory state as above mentioned. Then, cells were incubated with 0.5 mg mL<sup>-1</sup> of Cy5-psomes for 0.5, 1, 2, 4, 6, 12, 24, and 48 h, in a humidified atmosphere, 95% air, 5% CO<sub>2</sub> at 37 °C. After each incubation time point, followed by 3 steps of DPBS washing, cells were stained for CLSM live imaging. Respectively, for nuclear and cell membrane staining, Hoechst 33 342 (Sigma-Aldrich) and far-red Cell Mask (Life Technologies) were incubated for 10 min at room temperature, before visualization under CLSM. At least 10 different regions of the petri dishes were captured and analyzed using the Fiji ImageJ software (version 2.0). For the quantification of Cy5-psomes within stimulated macrophages and synoviocytes, their fluorescent intensity signal was normalized relative to the nuclear intensity signal.

**Cell Surface Receptors Quantification:** The cell scavenger receptor (SRB1 and SRB3 (commonly known as CD36) proteins expression levels in either non- or activated cells were detected by Western blotting assay. First, THP1 and HFLS were seeded at a concentration of 10<sup>6</sup> cells per well in 6-well plate (CytoOne) and then activated to the inflammatory state as above mentioned. After 24 h incubation in a humidified atmosphere, 95% air, 5% CO<sub>2</sub> at 37 °C, cells then washed with DPBS and lysed using radioimmunoprecipitation buffer (containing 50 mM Tris-HCl, pH 8.0, 1% Nonidet P-40, 150 mM NaCl, 0.5% sodium deoxycholate, 0.1% sodium dodecyl sulfate, 2 mM ethylenediaminetetraacetic acid, and 1 mM dithiothreitol) supplemented with protease and phosphatase inhibitor cocktails. Followed by centrifugation (12 000 g) at 4 °C for 10 min to remove the nuclei and any insoluble cell debris. The post-nuclear extracts were collected and used as total cell lysates. The protein concentration from these lysates was then determined following the Bradford assay kit protocol (Bio-Rad). Western blotting was performed as previously described with minor modifications.<sup>[59]</sup> Briefly, the cell lysates were first denatured in 4x Laemmli sample buffer (Bio-Rad) at 95 °C for 5 min. Then, 10  $\mu$ g of total cell lysates proteins were separated by electrophoresis on 10% SDS polyacrylamide gels (previously prepared following the Bio-Rad protocol) and transferred to a polyvinylidene difluoride (PVDF) membrane (Bio-Rad). The PVDF membranes were then blocked with 5% milk in Tris-buffered saline with 0.1% Tween-20 (TBST) for 1 h at room temperature. For the immunodetection of SRB1 and CD36 protein expression, the PVDF membranes were first incubated, overnight at 4 °C, with 1:1000 dilution of each specific primary antibody (Novus Biologicals NB400-144 and NB400-131) in 1% milk/TBST. And then, after several washes with TBST, the PVDF membranes were incubated with the secondary antibodies (1:20 000) in 1% milk/TBST for 1 h at room temperature. The signals of the goat anti-rabbit and anti-mouse IgG Dylight 800 (Invitrogen) were detected using the Odyssey CLx imaging system. The densitometry analyses were performed using Fiji ImageJ software (version 2.0), and the obtained values represent the ratio between the immunodetected protein and the glyceraldehyde 3-phosphate dehydrogenase (GAPDH, Abcam) loading control. Then, the fold change expression was determined by normalization to the non-activated control.

**Cell Viability Assay:** The thiazolyl blue tetrazolium bromide (MTT, Sigma-Aldrich) assay was used, as previously reported, to evaluate the cytotoxicity of all psomes formulations.<sup>[60]</sup> Briefly, for MTT assay, THP1 and HFLS were seeded at a density of 5 · 10<sup>3</sup> cell per well in 96-well plates (CytoOne). After seeding and activation, increasing concentrations of each treatment were incubated for 24 h in a humidified atmosphere, 95% air, 5% CO<sub>2</sub> at 37 °C. Control wells were incubated with equivalent volumes of corresponding cell culture medium and/or a solution of 10% (v/v) dimethyl

sulfoxide (DMSO, Sigma-Aldrich) in DPBS. Follow by 24 h incubation, 0.5 mg mL<sup>-1</sup> of MTT solution was added to each well, and 2 h later the MTT solution was replaced by the same volume of DMSO per well to dissolve the formed formazan crystals. Then, the optical density of solubilized blue crystals was read by measuring UV absorbance at 590 and 630 nm using a UV-vis microplate spectrophotometer (SynergyTM HT, Biotek). The cell viability was determined as the percentage of the metabolic activity of treated cells normalized to the control wells.

**NF- $\kappa$ B Signaling Imaging:** Nuclear factor- $\kappa$ B (NF- $\kappa$ B) signaling imaging was performed using CLSM. First, THP1 and HFLS were seeded at a concentration of 5 · 10<sup>4</sup> cells per glass-bottom petri dish (Ibidi) and activated as above mentioned. Then, 10  $\mu$ g mL<sup>-1</sup> of either free or MTX-loaded psomes was incubated for 24 h in a humidified atmosphere, 95% air, 5% CO<sub>2</sub> at 37 °C. Following treatment, cells were washed with DPBS and fixed using 3.7% formaldehyde (Sigma-Aldrich) for 10 min at room temperature. After the fixation step, followed by DPBS washing for the membrane permeabilization step, cells were incubated with 0.2% Triton-X (Sigma-Aldrich) for a further 10 min at room temperature. Then, the immunostaining blocking was performed using 5% bovine serum albumin (BSA) (Sigma-Aldrich), to prevent unspecific antibody binding. After 1 h at room temperature, cells were incubated with NF- $\kappa$ B p65 Antibody (F-6) Alexa Fluor 647 (SantaCruz Biotechnology) 1:500 diluted in 1% BSA overnight in a humidified chamber at 4 °C. The following day, cells were washed with DPBS and the nucleus was stained with Hoescht 33 342 (Thermo Fisher) for 10 min at room temperature, before visualization under CLSM. At least 10 different regions of the petri dishes were acquired. The NF- $\kappa$ B nuclear translocation imaging analysis was evaluated by co-localization (Pierce's coefficient values) of the NF- $\kappa$ B and nucleus fluorescence intensity signals using Fiji ImageJ software (version 2.0).

**Enzyme Linked Immunosorbent Assay:** The IL6 and TNF $\alpha$  protein levels were determined using an enzyme-linked immunosorbent assay (ELISA). First, THP1 and HFLS were seeded at a concentration of 10<sup>6</sup> cells per well in 6-well plate (CytoOne) and activated to the inflammatory state as above mentioned. Followed by 24 h incubation with 10  $\mu$ g mL<sup>-1</sup> of either free or MTX-loaded psomes in a humidified atmosphere, 95% air, 5% CO<sub>2</sub> at 37 °C. Afterward, supernatants of each treatment were then collected, and the ELISA (Invitrogen) was carried following the manufacturer protocol.

**Real-Time Quantitative Polymerase Chain Reaction:** Analyses on the gene expression of inflammation-related markers, including TNF $\alpha$ , IL1 $\beta$ , IL6, IL8, CCL3, and MMP13 was assessed using RT-qPCR. First, THP1 and HFLS were seeded at a concentration of 10<sup>6</sup> cells per well in 6-well plate (CytoOne) and activated as above mentioned. Followed treatment with 10  $\mu$ g mL<sup>-1</sup> of free or MTX-loaded psomes, for 6 and 20 h, respectively for macrophages and synoviocytes. Cells were then lysed, and the RNA was extracted following the RNeasy mini kit (Qiagen) protocol pre-installed in the QIAcube (Qiagen). The total ribonucleic acid (RNA) concentration was measured with NanoDrop spectrophotometer (ThermoScientific). Complementary deoxyribonucleic acid (cDNA) was synthesized from every 1  $\mu$ g of total mRNA in 20  $\mu$ L volume with QuantiTect Reverse Transcription Kit (Qiagen) according to the manufacture protocol. This procedure provided a fast and efficient cDNA synthesis with integrated removal of genomic DNA contamination. Briefly, the sample of RNA is incubated at 42 °C for 2 min to effectively remove containing genomic DNA, then the reaction occurred for another 15 min at 42 °C and then inactivated at 95 °C. RT-qPCR reaction was performed on yield cDNA synthesized from each sample using QuantiTect Rotor-Gene SYBR Green RT-PCR kit (Qiagen) using the Qiagility instrument software (Qiagen). This software enables rapid and high-precision system of sample preparation for RT-qPCR analysis, providing a step-by-step guidance for automatic calculation of all primers, cDNA template and Rotor-Gene SYBR Green master mixes need for the reaction. For the RT-qPCR experiments, the ribosomal protein L13A (RPL13A) and glyceraldehyde 3-phosphate dehydrogenase (GADPH) were used as reference genes, respectively for macrophages and synoviocytes. The list of designed primers of each target gene and reference gene are detailed in Table S3, Supporting Information. Following sample preparation, the PCR mixtures were placed in the Rotor-Gene Q cyclor (Qiagen) and amplification process started using the following protocol steps: Initial cycling step at 95 °C during 5 min for the DNA polymerase activation;

followed by 40 cycles of 95 °C during 5 s for denaturation; and 60 °C during 10 s for combined annealing and extension for all primers. RT-qPCR data analysis of folds-changes in gene expression levels normalized to the non-activated cells was determined by the  $-\Delta\Delta C_t$  method (details in SI), using cycle threshold ( $C_t$ ) values acquired from the amplification curve using the Rotor-Gene Q instrumentation software (Qiagen).

**Animal Experimental Design:** AIA 8-week-old female Wistar rats purchased from Charles River laboratories international (Spain) were housed in European type II standard filter top cages (Tecniplast) at the Specific Pathogen Free animal facility at the Institute of Molecular Medicine at the Faculty of Medicine, University of Lisbon. Here, the animals were individually identified and randomly housed in experimental groups of  $n = 5$ , as follows: i) AIA treated with MTX ( $0.223 \text{ mg kg}^{-1}$  body weight by daily intraperitoneal (i.p.) administration); ii) AIA treated with MTX-loaded psomes ( $0.223 \text{ mg kg}^{-1} \text{ day}^{-1}$  via i.p.); iii) AIA treated with psomes ( $10 \text{ mg kg}^{-1}$  body weight corresponding to the an equal mass of polymer injected in the (ii) group); the respective iv) AIA and v) non-arthritis healthy vehicle groups (received an equal volume of PBS). Daily i.p. injections in treated and vehicle groups started 4 days after disease induction, when the AIA Wistar rats already presented clinical signs of arthritis.<sup>[35]</sup> Experiments were approved by the Animal User and Ethical Committees, at the Institute of Molecular Medicine according to Portuguese law and European recommendations.

**Pharmacokinetics and Biodistribution:** Animals from both healthy and arthritic vehicle groups were injected intraperitoneally (i.p.) with Cy7-psomes polymersomes ( $10 \text{ mg kg}^{-1}$  body weight) at 24 h prior sacrifice. For pharmacokinetics analysis, blood samples were collected from the rat tail at several timepoints (0.5, 2, 4, 8, and 24 h) and immediately processed (centrifugation 2000 rcf for 10 min at 4 °C) for plasma separation from the blood cells. The plasma concentration of near infrared fluorescence of Cy7-psomes was measured using a multimode microplate fluorometer (Spark, Tecan, Switzerland). For the biodistribution study, 24 h post i.p. injection, the main organs (kidney, spleen, liver, and heart) were collected and wet weight and further fluorescence analysis of Cy7-psomes was accessed. Briefly, a part of the organ tissue was weight and homogenized following the protocol of the Precellys soft tissue lysing kit (CK14, Bertin Instruments, VWR, UK). The fluorescence of Cy7-psomes was measured in using a multimode microplate fluorometer (Spark, Tecan, Switzerland). Additionally, an in vivo imaging system (IVIS, Perkin Elmer) was used to evaluate the biodistribution of Cy7-psomes in the front and right hind paws of both healthy and AIA Wistar rats.

**Arthritic Inflammatory Signs:** Arthritic inflammatory signs in rats' paws and body weight were evaluated daily during the 15 days period of treatment. Inflammation scores were recorded following standard protocols and criteria established<sup>[35]</sup> by counting the score of each joint in a scale of 0–3, where: 0 = absence, 1 = erythema; 2 = erythema and joint swelling; 3 = deformities and functional impairment of the entire paw. The total inflammation score of each animal was defined as the sum of the partial scores of each affected joint. Additionally, the swelling of the hind paws was evaluated by measuring the ankle perimeter. In the end, all animals were then sacrificed 19 days post disease induction (15 days after treatment was started) where a maximum disease activity and severity occurs.<sup>[34]</sup> At the sacrifice time, animals were anesthetized with pentobarbital ( $100 \text{ mg kg}^{-1}$  body weight) administrated intraperitoneally. Here, the blood samples were collected by cardiac puncture and then processed (centrifugation 2000 rcf for 10 min at 4 °C) for further serum subsequent analysis. Afterward, the animal was perfused transcardially with PBS for vascular and organs hemoglobin release. The main organs (kidney, spleen, liver, and heart) and all paws were also collected and wet weight for further analysis.

**Histopathology:** Left hind paw samples were collected at the time of sacrifice and fixed immediately in 10% (v/v) neutral buffered formalin solution and then decalcified in 10% (v/v) formic acid. Samples were then dehydrated and embedded in paraffin, serially sectioned at a thickness of 4  $\mu\text{m}$  and then stained with haematoxylin and eosin (H&E) for histological analysis. The histopathological evaluation (by B.V.) of structural changes and cellular infiltration in paw sections was performed following previously reported criteria in a blind fashion using 5 semi-quantitative scores:<sup>[35]</sup>

Sublining layer infiltration score (0 = none to diffuse infiltration, 1 = lymphoid cell aggregate, 2 = lymphoid follicles, 3 = lymphoid follicles with germinal center formation); Lining layer cell number score (0 = fewer than three layers, 1 = three to four layers, 2 = five to six layers, 3 = more than six layers); Bone erosion score (0 = no erosions, 1 = minimal, 2 = mild, 3 = moderate; 4 = severe); Cartilage surface (0 = normal, 1 = irregular, 2 = clefts, 3 = clefts to bone); Global severity score (0 = no signs of inflammation, 1 = mild, 2 = moderate, 3 = severe). Additionally, sections of both liver and spleen of all experimental groups were as well stained with H&E and logically analyzed by an expert pathologist (S.B.).

**Serum Inflammation-Related Cytokines:** Serum levels of TNF $\alpha$ , IL1 $\beta$ , and IL6 were quantified using a specific rat ELISA (Invitrogen, Thermo Scientific) following the manufacturer protocol.

**Data Statistical Analysis:** Statistical analyses were performed using GraphPad Prism (version 8.2.1). Differences between groups were assessed by one-way or two-way ANOVA with Tukey multiple comparison test. The differences were statistically significant when  $*p < 0.05$ ,  $**p < 0.01$ ,  $***p < 0.001$ , and  $****p < 0.0001$ .

## Supporting Information

Supporting Information is available from the Wiley Online Library or from the author.

## Acknowledgements

V.M.G. thanks the received financial support from FCT (Fundação para a Ciência e Tencnologia) through the FCT Ph.D. Programmes and by POCH (Programa Operacional Potencial Humano), specifically by the Doctoral Programme on Cellular and Molecular Biotechnology Applied to Health Sciences for the grant (PD/BD/128388/2017). V.M.G. is also grateful to Diana Matias for her expertise and technical assistance with western blotting assay. C.N. also thanks FCT for the Investigator grant (IF/00293/2015) and respective exploratory project. G.B. thanks ERC for the consolidator award (CheSSTaG 769798), EPSRC Established Career Fellowship (EP/N026322/1), EPSRC/SomaNautix Healthcare Partnership EP/R024723/1, and Children With Cancer UK for the research project (16-227).

## Conflict of Interest

The authors declare no conflict of interest.

## Author Contributions

V.M.G. prepared and characterized the formulations, with A.P. and C.L.-V. contributed on the polymer synthesis and TEM, respectively. V.M.G. and L.R. designed and performed the in vitro experiments. V.M.G., L.R., and B.V. designed and performed the in vivo experiments, with E.S. and S.B. contributed on the IVIS and histological analyses, respectively. V.M.G., L.R., B.V., and C.N. contributed to data analysis and interpretation. V.M.G. prepared the figures and wrote the manuscript under the supervision of G.B., L.R., and S.R. and A.O., G.B., S.R., and A.O. supervised the research and contributed to the experiments design. All authors contributed substantially to the revisions of the manuscript and gave final approval for publication.

## Data Availability Statement

The data that support the findings of this study are available from the corresponding author upon reasonable request.

## Keywords

arthritis, inflammation, macrophage, methotrexate, polymersome, synovioocyte

Received: August 3, 2021  
Revised: December 15, 2021  
Published online:

- [1] S. A. Eming, T. A. Wynn, P. Martin, *Science* **2017**, *356*, 1026.
- [2] G. S. Firestein, *Nature* **2003**, *423*, 356.
- [3] J. S. Smolen, G. Steiner, *Nat. Rev. Drug Discovery* **2003**, *2*, 473.
- [4] V. Gouveia, S. Lima, C. Nunes, S. Reis, *J. Biomed. Nanotechnol.* **2015**, *11*, 1701.
- [5] M. P. van der Linden, S. le Cessie, K. Raza, D. van der Woude, R. Knevel, T. W. Huizinga, A. H. van der Helm-van Mil, *Arthritis Rheum.* **2010**, *62*, 3537.
- [6] U. Müller-Ladner, T. Pap, R. E. Gay, M. Neidhart, S. Gay, *Nat. Clin. Pract. Rheumatol.* **2005**, *1*, 102.
- [7] I. B. McInnes, G. Schett, *N. Engl. J. Med.* **2011**, *365*, 2205.
- [8] R. W. Kinne, B. Stuhlmüller, G. R. Burmester, *Arthritis Res. Ther.* **2007**, *9*, 224.
- [9] Z. Szekanecz, T. Besenyei, A. Szentpétery, A. E. Koch, *Curr. Opin. Rheumatol.* **2010**, *22*, 299.
- [10] C. X. Maracle, P. Kucharzewska, B. Helder, C. van der Horst, P. C. de Sampaio, A. R. Noort, K. van Zoest, A. W. Griffioen, H. Olsson, S. W. Tas, *Rheumatology* **2017**, *56*, 294.
- [11] E. Karouzakis, M. Neidhart, R. E. Gay, S. Gay, *Immunol. Lett.* **2006**, *106*, 8.
- [12] E. Choy, *Rheumatology* **2012**, *51*, v3.
- [13] R. Cascão, B. Vidal, I. P. Lopes, E. Paisana, J. Rino, L. F. Moita, J. E. Fonseca, *PLoS One* **2015**, *10*, e0142448.
- [14] R. S. Hardy, C. Hülso, Y. Liu, S. J. Gasparini, C. Fong-Yee, J. Tu, S. Stoner, P. M. Stewart, K. Raza, M. S. Cooper, M. J. Seibel, H. Zhou, *Arthritis Res. Ther.* **2013**, *15*, R24.
- [15] M. F. Bustamante, R. Garcia-Carbonell, K. D. Whisenant, M. Guma, *Arthritis Res. Ther.* **2017**, *19*, 110.
- [16] B. Bartok, G. S. Firestein, *Immunol. Rev.* **2010**, *233*, 233.
- [17] S. W. Tas, C. X. Maracle, E. Balogh, Z. Szekanecz, *Nat. Rev. Rheumatol.* **2016**, *12*, 111.
- [18] B. Bartok, D. Hammaker, G. S. Firestein, *J. Immunol.* **2014**, *192*, 2063.
- [19] A. Leblond, Y. Allanore, J. Avouac, *Autoimmun Rev.* **2017**, *16*, 594.
- [20] S. Lefèvre, A. Knedla, C. Tennie, A. Kampmann, C. Wunrau, R. Dinser, A. Korb, E. M. Schnäker, I. H. Tarner, P. D. Robbins, C. H. Evans, H. Stürz, J. Steinmeyer, S. Gay, J. Schölmerich, T. Pap, U. Müller-Ladner, E. Neumann, *Nat. Med.* **2009**, *15*, 1414.
- [21] I. B. McInnes, J. R. O'Dell, *Ann. Rheum. Dis.* **2010**, *69*, 1898.
- [22] S. S. Abolmaali, A. M. Tamaddon, R. Dinarvand, *Cancer Chemother. Pharmacol.* **2013**, *71*, 1115.
- [23] K. S. Upchurch, J. Kay, *Rheumatology* **2012**, *51*, vi28.
- [24] a) J. A. Wessels, T. W. Huizinga, H. J. Guchelaar, *Rheumatology* **2008**, *47*, 249; b) P. M. Brown, A. G. Pratt, J. D. Isaacs, *Nat. Rev. Rheumatol.* **2016**, *12*, 731.
- [25] K. Visser, D. M. van der Heijde, *Clin. Exp. Rheumatol.* **2009**, *27*, 1017.
- [26] V. M. Gouveia, C. Nunes, S. Reis, in *Nanoparticles in Life Sciences and Nanomedicine* (Eds: A. R. Neves, S. Reis), Pan Stanford Publishing, Pan Stanford Publishing Pte. Ltd, Singapore **2018**, Ch. 13.
- [27] a) H. E. Colley, V. Hearnden, M. Avila-Olias, D. Cecchin, I. Canton, J. Madsen, S. MacNeil, N. Warren, K. Hu, J. A. McKeating, S. P. Armes, C. Murdoch, M. H. Thornhill, G. Battaglia, *Mol. Pharmacol.* **2014**, *11*, 1176; b) C. Murdoch, K. J. Reeves, V. Hearnden, H. Colley, M. Massignani, I. Canton, J. Madsen, A. Blanazs, S. P. Armes, A. L. Lewis, S. Macneil, N. J. Brown, M. H. Thornhill, G. Battaglia, *Nanomedicine* **2010**, *5*, 1025; c) M. Massignani, I. Canton, T. Sun, V. Hearnden, S. Macneil, A. Blanazs, S. P. Armes, A. Lewis, G. Battaglia, *PLoS One* **2010**, *5*, e10459; d) L. Rizzello, J. D. Robertson, P. M. Elks, A. Poma, N. Daneshpour, T. K. Prajsnar, D. Evangelopoulos, J. O. Canseco, S. Yona, H. M. Marriott, D. H. Dockrell, S. J. Foster, B. D. Geest, S. De Kokexr, T. McHugh, S. A. Renshaw, B. Giuseppe, *bioRxiv* **2017**.
- [28] a) I. Canton, G. Battaglia, *Chem. Soc. Rev.* **2012**, *41*, 2718; b) L. Messenger, J. Gaitzsch, L. Chierico, G. Battaglia, *Curr. Opin. Pharmacol.* **2014**, *18*, 104.
- [29] a) J. B. El Khoury, K. J. Moore, T. K. Means, J. Leung, K. Terada, M. Toft, M. W. Freeman, A. D. Luster, *J. Exp. Med.* **2003**, *197*, 1657; b) Y. M. Park, *Exp. Mol. Med.* **2014**, *46*, e99.
- [30] a) N. Fujiwara, K. Kobayashi, *Curr. Drug Targets: Inflammation Allergy* **2005**, *4*, 281; b) Y. Oishi, I. Manabe, *Int. Immunol.* **2018**, *30*, 511.
- [31] S. Farnaghi, R. Crawford, Y. Xiao, I. Prasad, *Int. J. Rheum. Dis.* **2017**, *20*, 131.
- [32] M. F. Linton, H. Tao, E. F. Linton, P. G. Yancey, *Trends Endocrinol. Metab.* **2017**, *28*, 461.
- [33] K. Kannan, R. A. Ortmann, D. Kimpel, *Pathophysiology* **2005**, *12*, 167.
- [34] L. R. Schopf, K. Anderson, B. D. Jaffe, in *In Vivo Models of Inflammation* (Eds: C. S. Stevenson, L. A. Marshall, D. W. Morgan), Birkhäuser Verlag Basel, Switzerland **2006**.
- [35] a) R. Cascao, B. Vidal, H. Raquel, A. Neves-Costa, N. Figueiredo, V. Gupta, J. E. Fonseca, L. F. Moita, *Autoimmun Rev.* **2012**, *11*, 856; b) B. Vidal, R. Cascao, A. C. Vale, I. Cavaleiro, M. F. Vaz, J. A. Brito, H. Canhão, J. E. Fonseca, *PLoS One* **2015**, *10*, e0117100; c) B. Vidal, R. Cascao, M. A. J. Finnilä, I. P. Lopes, S. Saarakkala, P. Zioupos, H. Canhão, J. E. Fonseca, *PLoS One* **2018**, *13*, e0190920.
- [36] V. M. Gouveia, L. Rizzello, C. Nunes, A. Poma, L. Ruiz-Perez, A. Oliveira, S. Reis, G. Battaglia, *Pharmaceutics* **2019**, *11*, 614.
- [37] L. Guan, L. Rizzello, G. Battaglia, *Nanomedicine* **2015**, *10*, 2757.
- [38] J. D. Robertson, J. R. Ward, M. Avila-Olias, G. Battaglia, S. A. Renshaw, *J. Immunol.* **2017**, *198*, 3596.
- [39] a) M. A. Abdelhalim, *Biomed Res. Int.* **2013**, *2013*, 353695; b) I. Dirnena-Fusini, M. K. Åm, A. L. Fougner, S. M. Carlsen, S. C. Christiansen, *BMJ Open Diabetes Res. Care.* **2018**, *6*, e000560.
- [40] a) M. Massignani, C. LoPresti, A. Blanazs, J. Madsen, S. P. Armes, A. L. Lewis, G. Battaglia, *Small* **2009**, *5*, 2424; b) C. LoPresti, M. Massignani, C. Fernyhough, A. Blanazs, A. J. Ryan, J. Madsen, N. J. Warren, S. P. Armes, A. L. Lewis, S. Chirasatsin, A. J. Engler, G. Battaglia, *ACS Nano* **2011**, *5*, 1775.
- [41] H. Lomas, J. Du, I. Canton, J. Madsen, N. Warren, S. P. Armes, A. L. Lewis, G. Battaglia, *Macromol. Biosci.* **2010**, *10*, 513.
- [42] a) F. Fenaroli, J. D. Robertson, E. Scarpa, V. M. Gouveia, C. Di Guglielmo, C. De Pace, P. M. Elks, A. Poma, D. Evangelopoulos, J. O. Canseco, T. K. Prajsnar, H. M. Marriott, D. H. Dockrell, S. J. Foster, T. D. McHugh, S. A. Renshaw, J. S. Martí, G. Battaglia, L. Rizzello, *ACS Nano* **2020**, *14*, 8287; b) C. Pegoraro, D. Cecchin, L. S. Gracia, N. Warren, J. Madsen, S. P. Armes, A. Lewis, S. Macneil, G. Battaglia, *Cancer Lett.* **2013**, *334*, 328.
- [43] C. Contini, R. Pearson, L. Wang, L. Messenger, J. Gaitzsch, L. Rizzello, L. Ruiz-Perez, G. Battaglia, *iScience* **2018**, *7*, 132.
- [44] a) A. Lardner, *J. Leukocyte Biol.* **2001**, *69*, 522; b) T. Fukamachi, X. Wang, Y. Mochizuki, C. Maruyama, H. Saito, H. Kobayashi, *Int. Immunopharmacol.* **2013**, *17*, 148.
- [45] M. Narazaki, T. Tanaka, T. Kishimoto, *Expert Rev. Clin. Immunol.* **2017**, *13*, 535.
- [46] J. E. Fonseca, M. J. Santos, H. Canhão, E. Choy, *Autoimmun Rev.* **2009**, *8*, 538.
- [47] L. Skov, F. J. Beurskens, C. O. Zachariae, S. Reitamo, J. Teeling, D. Satijn, K. M. Knudsen, E. P. Boot, D. Hudson, O. Baadsgaard, P. W. Parren, J. G. van de Winkel, *J. Immunol.* **2008**, *181*, 669.

- [48] a) V. M. Gouveia, S. A. Lima, C. Nunes, S. Reis, *J. Biomed. Nanotechnol.* **2015**, *11*, 1701; b) L. D. Quan, G. M. Thiele, J. Tian, D. Wang, *Expert Opin. Ther. Pat.* **2008**, *18*, 723.
- [49] I. Treede, A. Braun, R. Sparla, M. Kuhnel, T. Giese, J. Turner, E. Anes, H. Kulaksiz, J. Fullekrug, W. Stremmel, G. Griffiths, R. Ehehalt, *J. Biol. Chem.* **2007**, *282*, 27155.
- [50] L. Wang, L. Chierico, D. Little, N. Patikarnmonthon, Z. Yang, M. Azouz, J. Madsen, S. P. Armes, G. Battaglia, *Angew. Chem., Int. Ed. Engl.* **2012**, *51*, 11122.
- [51] I. Canton, M. Massignani, N. Patikarnmonthon, L. Chierico, J. Robertson, S. A. Renshaw, N. J. Warren, J. P. Madsen, S. P. Armes, A. L. Lewis, G. Battaglia, *FASEB J.* **2013**, *27*, 98.
- [52] J. D. Robertson, L. Rizzello, M. Avila-Olias, J. Gaitzsch, C. Contini, M. S. Magoñ, S. A. Renshaw, G. Battaglia, *Sci. Rep.* **2016**, *6*, 27494.
- [53] J. Gaitzsch, M. Delahaye, A. Poma, F. Du Prez, G. Battaglia, *Polym. Chem.* **2016**, *7*, 3046.
- [54] C. Fetsch, J. Gaitzsch, L. Messenger, G. Battaglia, R. Luxenhofer, *Sci. Rep.* **2016**, *6*, 33491.
- [55] L. Ruiz-Pérez, L. Messenger, J. Gaitzsch, A. Joseph, L. Sutto, F. L. Gervasio, G. Battaglia, *Sci. Adv.* **2016**, *2*, e1500948.
- [56] L. M. Magalhães, C. Nunes, M. Lúcio, M. A. Segundo, S. Reis, J. L. Lima, *Nat. Protoc.* **2010**, *5*, 1823.
- [57] M. E. Lund, J. To, B. A. O'Brien, S. Donnelly, *J. Immunol. Methods* **2016**, *430*, 64.
- [58] H. C. Lin, T. H. Lin, M. Y. Wu, Y. C. Chiu, C. H. Tang, M. J. Hour, H. C. Liou, H. J. Tu, R. S. Yang, W. M. Fu, *PLoS One* **2014**, *9*, e107890.
- [59] D. Matias, L. G. Dubois, B. Pontes, L. Rosário, V. P. Ferrer, J. Balça-Silva, A. C. C. Fonseca, L. W. Macharia, L. Romão, T. C. L. S. E. Spohr, L. Chimelli, P. N. Filho, M. C. Lopes, J. G. Abreu, F. R. S. Lima, V. Moura-Neto, *Mol. Neurobiol.* **2019**, *56*, 1517.
- [60] V. M. Gouveia, J. Lopes-de-Araújo, S. A. C. Lima, C. Nunes, S. Reis, *Nanomedicine* **2018**, *13*, 1037.